

We are IntechOpen, the world's leading publisher of Open Access books Built by scientists, for scientists

6,900

Open access books available

186,000

International authors and editors

200M

Downloads

Our authors are among the

154

Countries delivered to

TOP 1%

most cited scientists

12.2%

Contributors from top 500 universities



WEB OF SCIENCE™

Selection of our books indexed in the Book Citation Index
in Web of Science™ Core Collection (BKCI)

Interested in publishing with us?
Contact book.department@intechopen.com

Numbers displayed above are based on latest data collected.
For more information visit www.intechopen.com



Enhanced Ulcer Recognition from Capsule Endoscopic Images Using Texture Analysis

Vasileios Charisis, Leontios Hadjileontiadis and George Sergiadis
Aristotle University of Thessaloniki
Greece

1. Introduction

The five senses constitute some of the most substantial elements of the human nature. Beyond their importance in daily life and perception of the world, they play crucial role in knowledge acquisition as well. For instance, medicine was one of the first domains where the conceptual tools of rationality and empiricism were combined with techniques of investigation to make the human body an object of knowledge (Foucault, 1973). In this context, the techniques mentioned above are based on the application of senses in order to acquire medical knowledge. More precisely, vision and hearing became specific objects of knowledge over the course of the 19th century, supplemented through technique and technology. Thus, seeing and hearing are to be understood as fundamentally and absolutely different modes of not only knowing the world, but also reaching a medical diagnosis.

A branch of medicine closely associated with one of these techniques, namely visual inspection, is gastroenterology. In the field of gastroenterology, vision is widely understood as the fundamental mode of knowing the state of the gastrointestinal (GI) tract. The advent of medical imaging technologies, such as radiography (in the wider sense), tomography and especially endoscopy, promoted this thesis (Lorenz *et al.*, 1993; Rutgeerts *et al.*, 1980) by enabling the visual examination without demanding to gain physical access. In case of visual inspection, as in case of auscultation, there are specific properties observed in order to assess the image content, no matter how simple or sophisticated the imaging technology is. During a stethoscope examination, for instance, the clinician attempts to identify frequency, pitch and duration deviations from the normal lung sounds. Similarly, during the observation of a medical image, there are image properties, corresponding to the acoustic ones of the pulmonary system, which may reveal the existence of illness. In the case of endoscopic GI tract images, these features essentially include texture, color and shape. The procedure that a clinician subconsciously follows in order to examine the images and reach a diagnosis is to seek for distortions. Distortions mainly in texture and color of the examined tissue, as compared to the features considered empirically or conceptually healthy. While color and shape are quite tangible approaches, the concept of texture is more abstract and subjectively defined and interpreted; however, embodies valuable information that can be used to identify or describe an image (Haralick *et al.*, 1973). The vagueness of this concept is evidenced by the fact that there is no universally agreed-upon definition of what image texture is and, in general, different researchers use different definitions depending upon the

particular area of application (Tuceryan & Jain, 1998). The most widely used and accepted definition of texture in the field of medical image analysis, which is also adopted in this chapter, is the one that defines texture as the spatial variation of pixel intensities. In other words, texture describes the relationship between the intensities of neighbouring pixels (not necessarily adjacent). Texture is a fundamental characteristic that entails substantial information about the structural arrangement of surfaces and their relationship to the surrounding environment. This information may be applied to estimate shape, surface orientation, depth changes and construction materials. Texture is an innate property of virtually all surfaces; the grain of the wood, the weave of a fabric, the pattern of crops in a field, rugae on the mucous membrane of the stomach, the mucosa of colon and small intestine. An example of various texture patterns is given in Fig. 1. This structural information has been proven crucial for medical image analysis and interpretation (Miller & Astley, 1992; Xie *et al.*, 2005). This is the case especially for gastroenterology where the internal mucous membranes of the digestive tract exhibit strong textural features and distinctive patterns. For instance, an eroded ulcerous region or a protruded cancerous tissue is visually distinguished, mainly, by its alternated texture. Another image property also important for abnormal tissue evaluation is color. Ulcers, for instance, exhibit greenish-yellow hues while an active bleeding spot is characterized by deep red tones. On the contrary, the normal intestinal mucous membrane is reddish-pink in color. Nevertheless, color cannot be utilized as a standalone objective modality for abnormal tissue detection, since it is not perceptually uniform. The perceived color is highly conditioned by the nature and the amount of ambient luminosity (Berlin & Kay, 1969). Despite the color constancy effect (Foster *et al.*, 1997) of the human color perception system, whereby the color perception of objects remains relatively constant under varying environmental and visual conditions, serious color variations and color casts exist because of the intervention of an endoscope or a camera between the intestinal tissue and the physician's eye. For these reasons, gastroenterologists use color and texture information together, as the visual clues, along with other complementary examinations (i.e., blood tests, urine tests etc.), in order to reach a diagnosis.

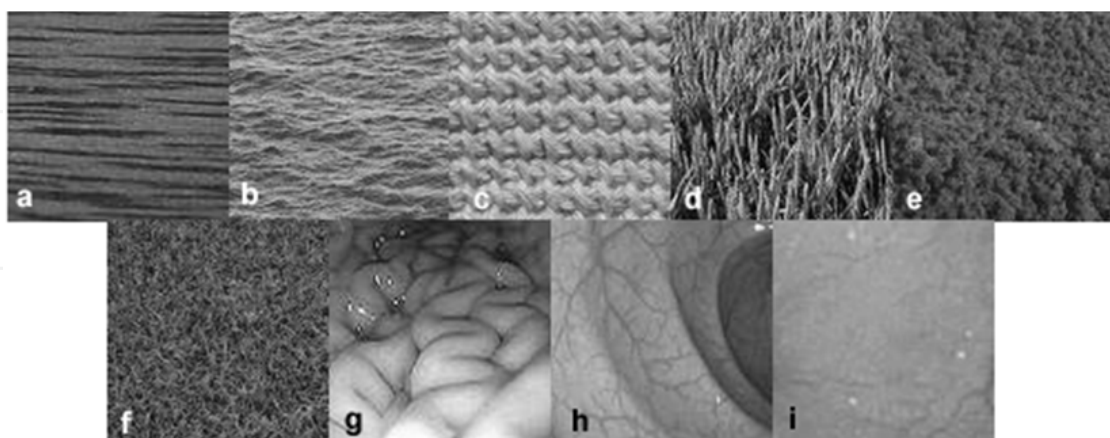


Fig. 1. Digital images with visibly different texture regions: a) grain of wood, b) water, c) cloth, d) corn cobs, e) forest, f) grass, g) stomach, h) colon, i) esophagus.

The advent of Wireless Capsule Endoscopy (WCE) and the gastroenterologists' requirement for faster and more secure diagnoses necessitated the development of effective intestinal-disorder recognition systems and automated WCE image analysis/inspection techniques.

The aim of WCE image processing techniques is to help the physician draw more reliable conclusions by generating enhanced and more informative images. During an examination with a stethoscope the physician instructs the patient how to breathe in order to get the best possible auscultation. In a similar way, a gastroenterologist who reviews an endoscopic video would desire the images to be as much informative as possible, but, without the opportunity to either give instructions to the patient or guide the capsule. The automated intestinal-disorder recognition systems target to detect potential regions of abnormal tissue in order to help the physician reach a diagnosis more quickly. This is particularly essential in WCE due to the vast amount of images produced (over 55,000) and the highly time-consuming task of reviewing them (more than two hours) (Maieron *et al.*, 2004). The fact that abnormal findings might not be clearly apparent to the naked eye further renders computer-aided image analysis imperative. It is not rare that abnormal findings are visible in only one or two WCE frames and easily missed by the physician. Additionally, contrast between malignant and normal tissue may be present but below the threshold of human perception. The human visual system fails to detect certain textured patterns. Julesz, an experimental psychologist, was an early pioneer in the visual perception of texture. He verified that human eye can discriminate textures that differ up to second order statistics (Julesz, 1975). In other words, a deliberate amount of effort is required to discriminate between two textures with identical second order statistics. Last but not least, the young age of WCE implies that most clinicians are inexperienced in this examination and automatic diagnostic systems could be great tools for those who wish to become experts in WCE. In this context, automatic inspection and analysis of WCE images is of immediate need.

From the aforementioned perspectives, it becomes clear that the auxiliary automatic diagnostic systems should exploit the texture and color features of the endoscopic images. Many efforts and computational approaches towards WCE image analysis have been reported in the literature. More specifically, researchers are concerned with malicious tissue detection which refers to detection of abnormal regions, such as tumors, polyps, bleeding and ulcer. To cope with this matter, traditional pattern recognition methods are applied, utilizing both chromatic and achromatic image domains. In particular, detection of abnormal patterns is achieved by employing local color features (Li & Meng, 2007), texture unit number (NTU) transformation and texture spectrum (Kodogiannis *et al.*, 2007a, 2007b) and synergistic methodologies, such as L-G graphs and image registration (Bourbakis, 2005). Local binary patterns (Iakovidis *et al.*, 2006) with the aid of G-statistic (Wang *et al.*, 2006), co-occurrence matrices (Ameling *et al.*, 2009), and discrete wavelet transform in conjunction with second-order statistics (Karkanis *et al.*, 2007; Magoulas, 2006) contributed to polyp and tumor detection. Regarding ulcer recognition, the related research is quite limited, no matter how common and important this disease is. The techniques proposed include feature extraction from a curvelet-based uniform local binary pattern (Iakovidis *et al.*, 2006; Li & Meng, 2009b), chromaticity moments calculated with the aid of Chebychev polynomials (Li & Meng, 2009a), texture spectrum (Kodogiannis *et al.*, 2007b), MPEG-7 descriptors (Coimbra & Cunha, 2006) and Red-Green-Blue (RGB) pixel values evaluation (Gan *et al.*, 2008). However, their success rate is limited.

This chapter sheds light upon one of the main issues of the WCE image analysis field, i.e., the overall detection enhancement of one of the most common diseases in the GI tract, namely ulcer; hence, enriching the inadequate existing literature. This goal is achieved by emphasizing on efficient elicitation of the structure characteristics of ulcerations and by

introducing new feature vectors (FVs). In particular, this chapter describes the use of innovative computer vision approaches towards the evaluation of ulcer-related content of WCE images. These approaches are similar to those employed by physicians in clinical practice to reach a diagnosis, i.e., the concept of color-texture characteristics. More specifically, they include sophisticated image processing tools with robust mathematical background, drawn from the field of Multi-Resolution Analysis, resulting in discrimination between ulcer and healthy regions. Additionally, innovative feature extraction algorithms, structured in both space and space-frequency domains, are presented, along with their application to real WCE data, collected from patients with ulcerous diseases. The chapter concludes by pointing out the potential of the proposed approaches towards efficient automated ulcer detection systems that will moderate the labour of the gastroenterologist and, consequently, the cost of the WCE examination.

2. Wireless Capsule Endoscopy (WCE)

In gastroenterology, the most common and established technique to visually inspect the GI tract and diagnose its diseases is endoscopy. The traditional endoscopic examinations applied for diagnosis in the upper and lower part of the GI tract, including esophagus, stomach, duodenum, terminal ileum and colon, are highly invasive causing discomfort to the patients. The visual inspection of the entire small intestine, in particular, has posed a challenge to gastroenterologists due to the strain of physically reaching it. Its important length and numerous windings make the examination extremely difficult, painful and not always possible, since usually there is a dead space in the middle part. Some imaging techniques used for the small intestine inspection include enteroclysis, small bowel follow through, push, sonde, and double balloon enteroscopy. Nevertheless, they are deeply inconvenient for the patients and require highly experienced gastroenterologists.

In 2000, advances in high integration and miniaturization allowed the researchers of Given Imaging to draw the attention of the GI community by unveiling what is now called endoscopic capsule. Wireless capsule endoscopy (WCE) (Iddan *et al.*, 2000) is a novel medical procedure, which has revolutionized endoscopy, as it has enabled, for the first time, a painless and effective diagnosis inside the GI tract. A WCE system consists of the capsule endoscope, a data recorder system and computer software for WCE data processing. The capsule endoscope is a disposable, pill-shaped device which consists of a CMOS camera, four light sources, two batteries and a radio transmitter. The patient shallows the capsule which captures images of the GI tract at a speed of two frames per second (fps). These images are compressed with JPEG algorithm and transmitted wirelessly to a special recorder attached to the patient's waist. The entire process lasts approximately 8 hours until the batteries exhaust. Finally, the images stored in the recorder are downloaded to a computer and the physicians, with the aid of the special software, can review the images and analyse potential sources of various GI diseases. The capsule travels along the digestive tract with the physiological peristalsis, without the need for air insufflation and sedation. Thus, the examination of the entire small intestine has become the most comfortable endoscopic examination for the patient to undergo. In this way WCE is suitable even for children and elderly.

WCE has proven invaluable in evaluating various diseases of the small bowel (Friedman, 2004; Pennazio, 2005), such as obscure bleeding (Mylonaki *et al.*, 2003), polyps and neoplasm, Crohn's disease, celiac disease and mucosal ulcers (Aronott & Lo, 2004). Ulcer is

one of the most common lesions of the GI tract that affects approximately 10% of the people. The most usual causes are *Helicobacter pylori* bacteria and use of nonsteroidal anti-inflammatory drugs (NSAID). Ulcer is a chronic inflammatory sore or erosion on the internal mucous membranes that arises in small intestine, especially in duodenum (the upper part of the small intestine) and in stomach. Some serious diseases are associated with ulcer, like Crohn's disease and ulcerative colitis. Although ulcer by itself is not lethal, complications are capable of causing death. That is the reason why early diagnosis and treatment is extremely essential.

2.1 Side effects

WCE is a well-tolerated and safe procedure with very few and rare complications. The main risk of WCE is capsule retention. Despite the small diameter of the capsule, a narrowing of the small bowel may cause it to become retained at a site of stricture. However, retention is estimated to occur in less than 1% of cases (Liao *et al.*, 2010). The 2005 International Conference on Capsule Endoscopy reached a consensus stating that a capsule would be deemed to have been retained if it could be shown to be remaining in the GI tract more than two weeks, without symptoms, after it had been ingested. The causes of capsule retention are bowel obstructions narrower than the size of the capsule (11mm diameter). Small bowel strictures are a frequent complication of Crohn's disease (Cheifetz *et al.*, 2006) and prolonged use of NSAID (Meredith *et al.*, 2009). The risk of capsule retention is also high for patients with a history of bowel obstruction or a previous gastrointestinal surgery. In case of retention, the removal of the capsule is most commonly performed by surgery (Barkin & Friedman, 2002), often resecting the obstructing lesion at the same time. However, there are cases where the removal is possible with traditional endoscopic techniques.

In order to reduce the risk of retaining the capsule, a barium small bowel examination should be performed or a biodegradable patency capsule (Fig. 2) (Riccioni *et al.*, 2003) should be digested prior to WCE. However, two studies (Meredith *et al.*, 2009) indicated that small bowel follow through radiography (SBFT) investigations were not effective at excluding patients at risk of retention. Additionally, patients with abnormal SBFT can have successful WCE. The patency capsule is exactly the same size as the capsule endoscope but it is made from lactose, with 10% barium sulphate to make it radiopaque, and surrounded by

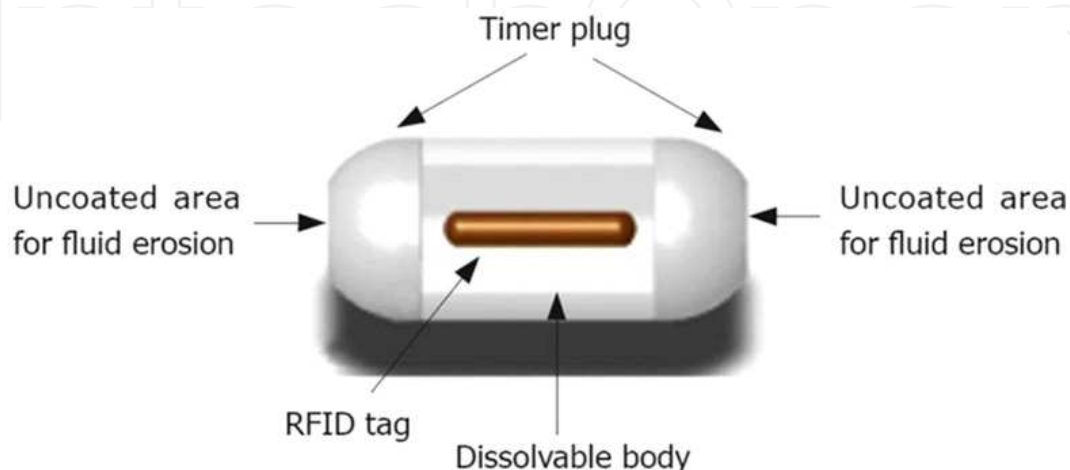


Fig. 2. Schematic drawing of a biodegradable patency capsule.

a cellophane coating. It has a timer plug which is slowly dissolved by gastric fluids, giving a disintegration time of 40-100 hours post ingestion, and contains a very small radiofrequency identification tag (RFID) which can be used to track its location in the small bowel without the use of ionizing radiation. The patency capsule remaining in one area for a large period of time can suggest retention. Early experience with this biodegradable capsule indicates that it allows accurate and objective evaluation of potentially obstructing small bowel lesions prior to WCE (Belvin *et al.*, 2003; Cauendo *et al.*, 2003). Although the patency capsule is mostly soluble, there needs to be further research to determine whether its use will reduce the risk of the patient, requiring surgery to remove there is a pathological stricture present. Successful passing of this patency capsule intact and without pain can provide evidence that a capsule endoscope will have a similar successful journey.

To conclude, the retention of a capsule endoscope can be a significant complication procedure, requiring corrective surgery. Whilst the overall risk of retention is low, factors that increase this risk include known or suspected Crohn's disease, a history of NSAID use and previous small bowel surgery. Taking a careful medical history can identify those patients at higher risk of retention, and for those identified, the administration of a patency capsule allows the assessment of the patient's risks from swallowing a small bowel WCE.

2.2 Advances in wireless capsule endoscopy

WCE is still an under development technology, which may change endoscopy forever. However, there are technical limitations that raise some serious questions. Will capsule endoscopy replace traditional upper gastrointestinal endoscopy and colonoscopy? Will capsule endoscopy be able to deliver therapy? The answer is probably yes, but, there are major challenges that the capsule technology needs to overcome, to compete with probe gastroscopy and colonoscopy. As mentioned before, WCE is especially recommended for exploration of the small bowel, while it exhibits poorer diagnostic efficacy for the examination of esophagus, stomach and colon (Van Gossum *et al.*, 2009). The limitations/challenges include: power management, camera speed and image quality, controllable manoeuvring, and interventional capabilities (Swain, 2008).

The first endoscopic capsule, due to limited power supply, ceased image capturing before crossing the entire GI tract. It was even possible that transmission stopped before the end of ileum, in case of extended residence in stomach. Consequently, visualization of colon was impossible. In this context, researches were directed towards a more energy efficient capsule, capable of exploring the entire digestive tract. Technological advances allowed researchers to make radical changes in WCE design and energy supply (Moglia *et al.*, 2009). In particular, two breakthroughs took place. Firstly, the advent of more efficient battery materials (i.e., carbon nanotubes and buckytubes) led to batteries smaller in size with better electrical conductivity leaving room for a third battery in the capsule with a slight increase in size. Secondly, an intelligent power management system was introduced in the data recorder that saves energy by regulating the image transmission rate and applying a sleep mode to the capsule. The recorder recognizes the location of the capsule inside the GI tract and adjusts the transmission rate accordingly. The capturing of images starts half an hour after ingestion to allow travelling to the target area (sleep mode). When the capsule arrives in stomach, the recorder recognizes it and maintains a slow transmission rate of six images per minute. The recorder is also able to detect when the capsule enters small intestine and

raises the transmission rate. Additionally, the recorder identifies if the capsule is in motion or stationary. If the capsule is moving the camera captures up to 35 images per second. Last but not least, the recorder has the intelligence to notify the patient with a sound signal and a vibration to ingest a prokinetic agent if the capsule resides in stomach for over an hour. This new design and technical achievements are very impressive. Yet the critical question to be addressed is whether this new capsule endoscope leads to improved diagnostic performance compared to traditional colonoscopy. Studies (Adler & Metzger, 2011) indicate that the diagnostic yield of WCE in colon has increased but still cannot surpass colonoscopy.

Currently, researchers intensely strive to unravel the issue of limited energy store inside the capsule by developing external wireless power transmission systems (Carta *et al.*, 2010). These approaches are based on magnetic fields and three-dimensional (3D) coils through a process that is known as inductive coupling. According to this phenomenon, an alternating magnetic field induces electrical voltage and electrical current to a coil that resides inside the field. Thus, the concept is to create a magnetic field around the human body that will transmit power to the capsule. To accomplish this, the capsule is equipped with windings of very thin copper wires (Fig. 3) around a ferrite core towards all three directions (3D coil). Ferrite is a lightweight material with efficient electromagnetic characteristics that support the formation of magnetic field. The existence of a ferrite core inside a coil has the effect of locally intensifying the magnetic field; hence, increasing the amount of collected power. On the contrary, the absence of the ferrite core would necessitate a larger coil for the same amount of received power. External power transmission systems seem promising and safe. Over 300mW usable power can be delivered while the maximum specific adsorption rate (SAR) does not exceed 0,329 W/Kg (Xin *et al.*, 2010), under the basic restrictions of the International Commission on Non-ionizing Radiation Protection (ICNIRP). However, there are major issues to deal with. The orientation of the capsule inside the body highly affects the stability of the received power. The amount of received power may drop over 55% for specific orientations which affects the proper operation of the capsule. Moreover, there is extensive power loss (over 70mW) in the electronic circuit that accompanies the coil inside the capsule. Another, equally important, problem is the stability of the external magnetic field which is altered by the human body. Despite the aforementioned issues, great steps forward have been made and it is likely, in the near future, an externally powered capsule endoscope to be realized.

The development of imaging technology and miniaturization resulted in size reduction of the image sensors and expansion of the camera angle of view. A wider viewing angle means



Fig. 3. 3D coil inside capsule endoscope for wireless power transmission (Carta *et al.*, 2010).

more panoramic images. Smaller cameras contributed to increased free space inside the capsule, and as a result, the inclusion of a second camera. The twin camera capsule with a wider angle of view combined with the increased transmission frame rate enabled esophageal WCE (Waterman & Granlnek, 2009) with promising diagnostic efficiency. The size reduction of image sensors is, also, expected to result in increasing number of pixels and solve the problem of low resolution WCE images. New and more efficient image compression algorithms will, additionally, assist towards quality and color enhancement. Image compression is essential in WCE in order to significantly reduce the size of the image and, consequently, the storage space and transmission time required. However, the compression procedure lowers image quality by smoothing the razor-sharp details.

Gastroenterologists eagerly look forward the day that they will be able to control and steer the capsule endoscope as they do in standard endoscopy. This would give them control in maintaining the capsule steady in selected areas and hold the view in order to examine carefully the opposite wall of the bowel. To solve this problem, magnetic manoeuvring has recently become a thrust research area. The proposed approaches rely on a magnetic field applied to the capsule from the exterior of the patient, exploiting the principle that a magnet inside a magnetic field aligns with the direction of the field. The magnetic field can be used to control the movement trajectory, the position and the orientation of the endoscopic capsule. By changing the direction of the magnetic field, the direction of the capsule also changes. For this purpose, various techniques have been proposed in order to make an endoscopic capsule responsive to an external magnetic field. These include either magnetic parts and induction coils to be arranged inside the capsule, or magnetic shells to be reversibly applied to the capsule externally (Capri *et al.*, 2007) (Fig. 4). Capsule motions can readily be induced with hand-held/hand-guided magnets, as demonstrated even in the esophagus and stomach of a volunteer (Swain, 2010). This system is only available for research purposes. Nevertheless, the main issue related to the development of a clinically applicable technique is the generation and precise control of a stable magnetic field, really capable of guaranteeing accurate and reliable manoeuvrings of an endoscopic capsule. Such techniques start to emerge (Capri *et al.*, 2011; Gao *et al.*, 2010) and the realization of a self-propelled capsule is close.



Fig. 4. Capsule with magnetic shield for controllable maneuvering (Capri *et al.*, 2011).

At present, WCE remains just a diagnostic tool that has yet to prove its potential. The endoscopic capsule is passive and cannot obtain biopsies, aspirate fluid, deliver drugs or brush lesions for cytology. The main pressure is to reduce the capsule size, which will

release space that could be used for other interactive functions, and maximize power supply. New engineering methods for constructing tiny moving parts, miniature actuators and even motors into capsule endoscopes are being developed. However, these moving components require considerable amounts of power. Another limitation to therapeutic capsule endoscopy is the low mass of the capsule endoscope (approximately 4 grams). A force exerted on tissue, for example, by biopsy forceps may push the capsule away from the tissue. Opening small biopsy forceps to grasp tissue and pull it free will require different solutions to those used at conventional endoscopy. All these interventional capabilities seem to be something of a pipe dream at present but the huge technological leaps pave the way for an active therapeutic capsule.

The ideal WCE of the gastroenterologist's imagination should be remote controlled and capable of performing an ordinary biopsy as well as stop bleeding using adrenaline injection or a heat probe. The ultimate capsule would include special detectors for white blood cells and be able to measure various cytokines, pH, temperature and pressure, in addition to delivering drugs. Finally, the optimal WCE needs to contain a computerized system for automatic detection of pathologies, such as ulcer and polyps, in order to overcome the drawback of time-consuming viewing the video (Fireman, 2010). Technology for improving the capability of the future generation capsule is almost within grasp and it would not be surprising to witness the realization of these giant steps within the coming decade.

3. The concept of image decomposition

Automated knowledge extraction from medical images is a fast growing field of interest for the researchers. The attainment of this objective requires image decomposition to its components that will disclose the inherent structural characteristics of the image. In this context, this section presents Bidimensional Ensemble Empirical Mode Decomposition, a novel tool for image analysis.

3.1 Empirical Mode Decomposition (EMD)

In 1998, Huang *et al.* introduced a novel, intuitive and alternative signal decomposition technique for time-frequency analysis, namely Empirical Mode Decomposition (EMD) (Huang *et al.*, 1998). The major characteristic of EMD that renders it superior to traditional analysis methods, such as Fourier and Wavelets, is its adaptive nature. The decomposition does not require the use of *a priori* basis function. On the contrary, it is totally data driven. The concept that lies behind EMD is the existence of oscillations in every signal, at a very local level. Therefore, its target is to seek and reveal these inherent oscillatory modes, called Intrinsic Mode Functions (IMFs). EMD is designed to estimate IMFs of a signal so that, no matter how complicated the signal is, it embeds. A given signal $x(t)$ can be decomposed into n IMFs as:

$$x(t) = \sum_{i=1}^n c_i(t) + r_n(t), \quad (1)$$

where $c_i(t)$ is i^{th} IMF (IMF i) and $r_n(t)$ is the low frequency trend of $x(t)$ (residue). The highest frequency component of $x(t)$ corresponds to the lowest value of index i , i.e., $c_1(t)$ (IMF 1).

While the value of i increases, lower frequency components are obtained. An example is given in Fig. 5a, where the signal is decomposed into five IMFs plus residue. The process to calculate each $c_i(t)$ is called sifting process. The local extrema are defined and interpolated, resulting in two fitting curves, one for the maxima and one for the minima. Then, the mean curve is calculated and subtracted from the signal. This procedure continues until a stopping criterion is satisfied. The signal that remains after the last subtraction is $c_1(t)$. Next, $c_1(t)$ is subtracted from the initial signal and the remainder constitutes the new initial signal on which the above procedure is applied in order to extract the following IMFs until the desired number is obtained.

3.2 Ensemble EMD (EEMD)

Despite the great advantage of EMD, deficiency arises when the extrema of the original signal are unevenly distributed. In such a case, the IMFs are incorrectly calculated, since either a single IMF contains signals of widely disparate scales or a single mode of oscillations resides in two or more IMFs. This phenomenon is called *mode mixing* and an example is depicted in Fig. 5b. It is clear that the first two IMFs, apart from the high frequency component of the signal, incorrectly include a low frequency oscillation. To overcome this issue, Huang *et al.* proposed a noise-assisted version of EMD, namely ensemble EMD (EEMD) (Wu & Huang, 2009). EEMD requires the generation of an ensemble that contains multiple copies of the original signal that are distorted by white Gaussian noise, different for each copy, of finite amplitude. EMD is applied on every member of the ensemble and the final IMFs of the initial signal are derived by averaging the corresponding IMFs of each member of the ensemble. The concept of EEMD is grounded on the intuitive characteristics of white noise. White noise populates the whole time-frequency space uniformly and, as a result, establishes proper reference scales for the IMFs. The inherent modes of the signal are triggered by the noise and are projected accurately on the correct

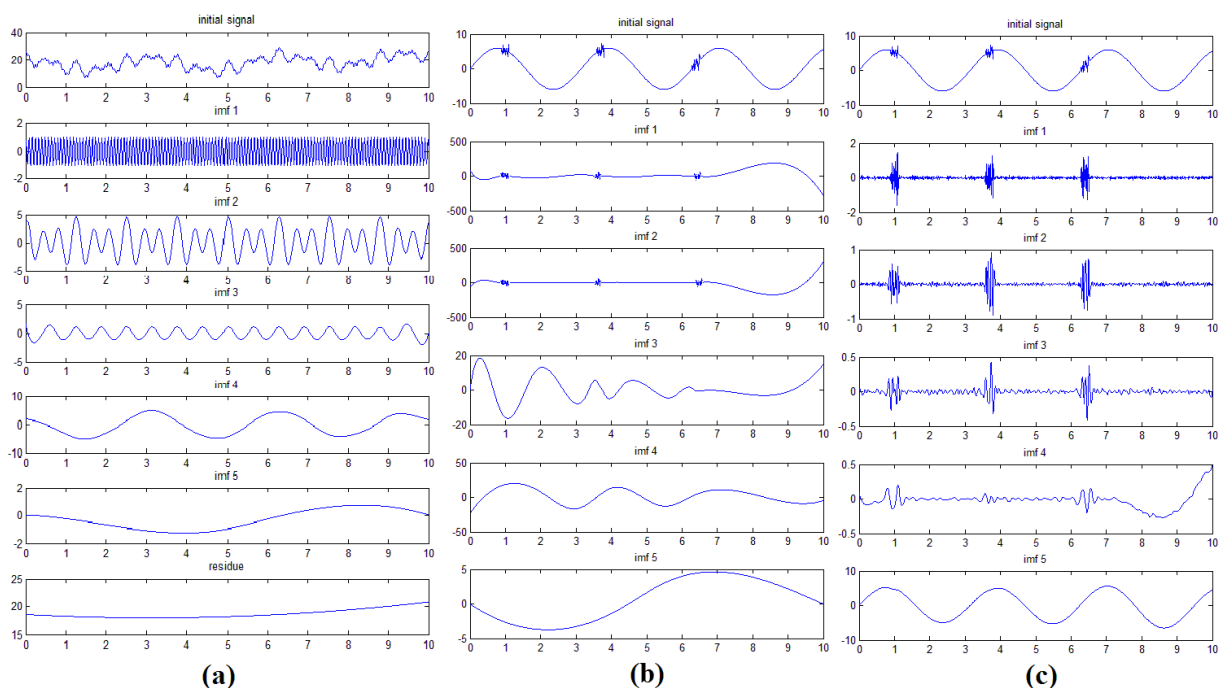


Fig. 5. (a) EMD analysis, (b) mode mixing phenomenon, (c) ensemble EMD analysis.

scales. The IMFs of each ensemble member are noisy but the final average IMFs are noise-free, since white noise cancels itself for a large number of ensemble members. Figure 5c presents the correct decomposition (using EEMD) of the signal in Fig. 5b. IMFs 1-3 include only the high frequency components while IMF5 contains the sinusoidal oscillation of the initial signal.

3.3 Bidimensional EEMD (BEEMD)

A multidimensional approach of EMD is required in case of a multidimensional signal. The extension of EMD in two dimensions (2D), namely Bidimensional EMD (BEMD), is an alternative multi-resolution analysis technique for image analysis and pattern discrimination. BEMD decomposes a 2D signal in 2D IMFs in the same way as eq. (1) demonstrates. However, there are two approaches for the realization of 2D extension. The first approach treats 2D data (images) as a collection of 1D slices (rows/columns) and applies 1D EMD on each row/column of the image (pseudo-BEMD). The second approach directly transplants the idea of 1D EMD algorithm in 2D data (genuine BEMD) after applying the appropriate changes (for example, fitting surfaces replace fitting curves). The first approach has the advantage of higher speed, while the latter exhibits improved performance, since the correlation among rows/columns of the image is taken into account. Bidimensional EEMD is the extension of EEMD in 2D (Wu *et al.*, 2009).

4. Texture extraction

Texture is a major property of any image that is useful in machine vision applications, especially for medical purpose. There are many approaches for texture analysis proposed in the literature. This paragraph describes the concept of Differential Lacunarity, an efficient tool for texture features extraction and identification.

4.1 Lacunarity Analysis (Lac)

Lacunarity (Lac) was introduced by Mandelbrot (Mandelbrot, 1993) as a fractal property, counterpart to fractal dimension (Mandelbrot, 1982), that describes the texture of a fractal. *Fractal dimension* is a measure of how much space is filled without consideration about the space-filling characteristics of data. In other words, two datasets with identical fractal dimensions can have distinct patterns with great differences in appearance. The introduction of Lac addressed this issue. Lac analyzes *how space is filled and consequently, can discriminate textures and natural surfaces that share the same fractal dimension*. In this direction, Lac has been used as a general technique to analyze patterns of spatial dispersion (Plotnick *et al.*, 1996). The term "lacunarity" has been used to evaluate and describe the distribution of gap sizes along datasets. A set with gaps of widely disparate sizes is considered heterogeneous and is characterized by high Lac, while a homogeneous set, with uniform gap sizes, exhibits lower Lac. It should be highlighted that homogeneous sets at large scales can be quite heterogeneous when examined at smaller scales and vice versa. From this perspective, Lac can be considered as a scale dependent tool to measure the heterogeneity or texture of an object (Gefen *et al.*, 1983).

Various algorithms have been proposed to calculate and quantify Lac, but the most popular are based on the "gliding box algorithm" (GBA) (Allain & Coitre, 1991) that is

straightforward and computationally simple. GBA is applicable on binary datasets, although it can be extended to real datasets by converting the numerical data to dyadic by thresholding (Plotnick *et al.*, 1996).

4.2 Differential Lacunarity Analysis (DLac)

Most real life, image analysis applications need to extract texture information from either grayscale or color images without the option of thresholding. To this end, Dong (Dong, 2000) introduced a new version of Lac, namely Differential Lacunarity (DLac), suitable for grayscale image analysis. DLac is calculated by a differential box counting method. This algorithm employs a gliding box r of size $r \times r$ pixels and a gliding window w of size $w \times w$ pixels with $r < w$. Window w is initially positioned at the up left corner of the image and, by moving one by one columns to the left, scans the whole image. For every position of the window w , box r is placed inside the window at the up left corner and scans the image pixels bounded by the window (Fig. 6a) in order to calculate a value called "box mass". In other words, window w designates a region of the image (different each time until the entire image is covered) on which box mass is calculated with the aid of box r . According to the pixel values included in the box ($r \times r$ neighborhood) a column of more than one cubes of size ($r \times r \times r$) may be needed to cover the image intensity surface (Fig 6b). Numbers 1, 2, ... are assigned to the cubes from bottom to top and the differential height of the column $n(i,j)$ is calculated (i, j is the position of the box). Let the minimum and maximum pixel values reside in the cubes u and v , respectively. The differential height of the column is defined as

$$n(i,j) = v - u - 1. \quad (2)$$

As the box glides inside the window, the sum

$$M = \sum_{i,j} n(i,j), \quad (3)$$

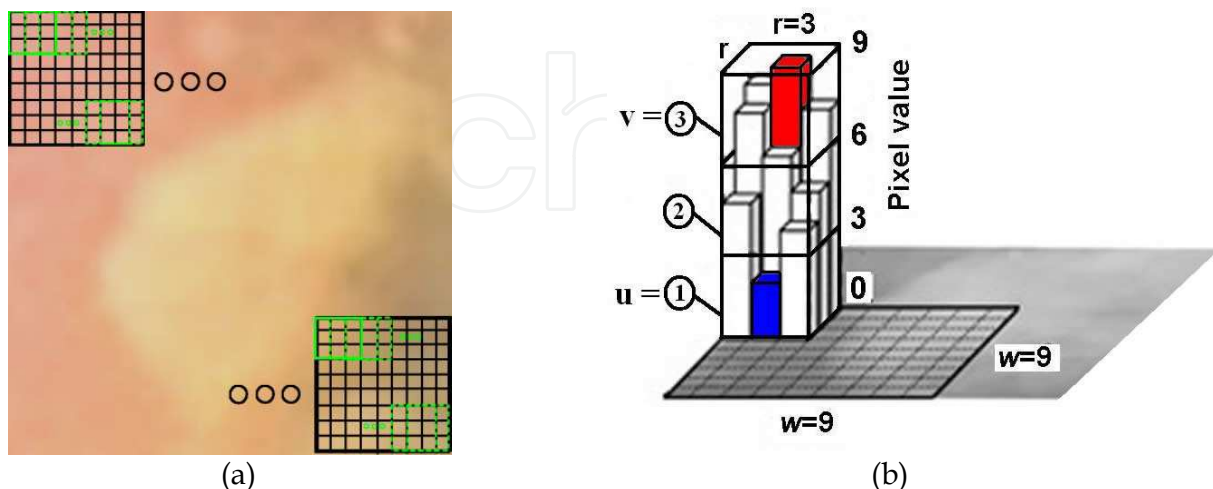


Fig. 6. (a) gliding box (green) and gliding window (black) movement throughout the image, (b) differential box counting method for box mass calculation (box size $r=3$, window size $w=9$, differential height of the column $n=3-1-1=1$).

is the box mass of the window w at a specific place. Let $n(M,r)$ be the number of windows w with box mass M calculated by a box r . The probability function $Q(M,r)$ is obtained by dividing $n(M,r)$ by the total number of windows. The DLac of the image at scale r given a window w is defined as

$$\Lambda(r) = \frac{\sum_M M^2 Q(M,r)}{[\sum_M M Q(M,r)]^2} \quad (4)$$

5. The proposed automated ulcer tissue identification scheme

This section presents our proposed approach for color-texture-based automatic discrimination between ulcer and healthy tissue from WCE images. The color-texture concept was motivated by gastroenterologists' clinical practice, where the colour and texture properties of WCE images are utilized for reaching a diagnosis. More specifically, our scheme, named AR-DLac, combines BEEMD analysis to achieve adaptive image refinement (AR) with DLac analysis for efficient extraction of ulcer texture information. BEEMD-DLac combination for WCE image analysis was firstly introduced in (Charisis *et al.*, 2010b). The overall structure of the propose scheme is depicted in Fig. 7.

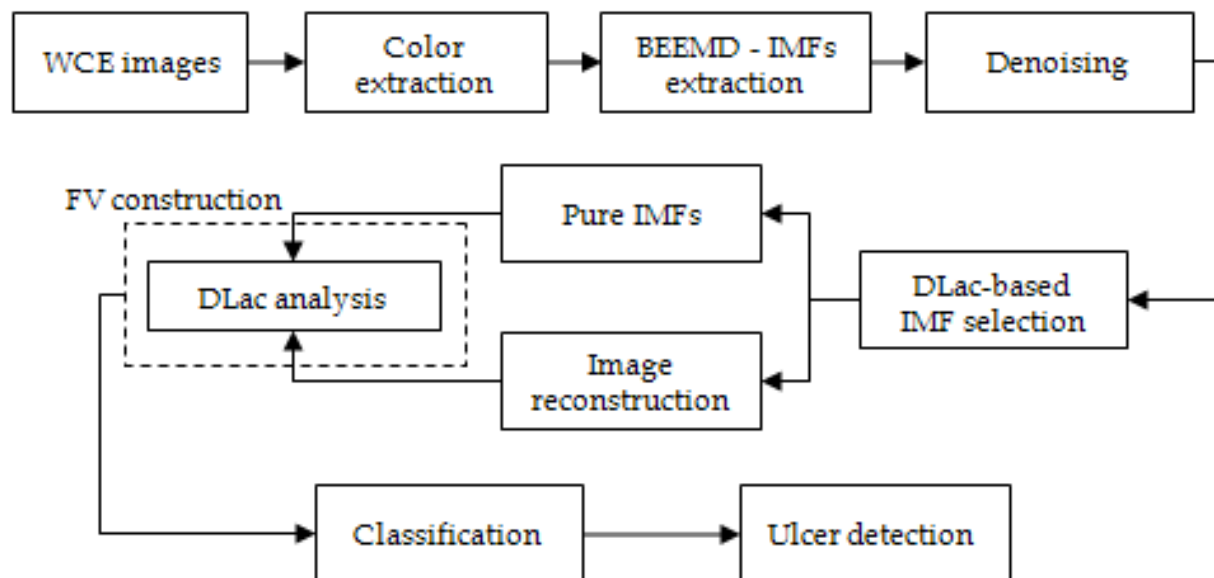


Fig. 7. The proposed AR-DLac scheme.

5.1 Color information

Each pixel in an image is characterized by a 3D color vector, i.e. three values that determine the color of the pixel. Various colour spaces exist to represent colour information. One of the most common color spaces is the hardware-oriented RGB (Red-Green-Blue). The majority of digital cameras, including the camera of a WCE system, utilize image sensors that capture colour images on the basis of the RGB model. In RGB, each colour is determined by the amount of red (R), green (G) and blue (B) present in the colour. In this context, a coloured WCE image comprises from three monochromatic components, one for each colour (R, G and B), whose combination provides the final colourful image.

Previous studies (Charisis *et al.*, 2010a, 2011) have shown that RGB is the most efficient space for WCE image analysis (compared to other colour spaces, i.e., HSV and CIE Lab). More specifically, the majority of ulcer texture information resides in green component of the RGB space. This conclusion coincides with the yellow-greenish appearance of ulcer regions. Thus, the proposed AR-DLac scheme is applied on the green channel extracted from each image.

5.2 Image denoising

The next step of our approach includes image purification by applying a denoising procedure. In order to facilitate texture-pattern extraction, the images need to be refined and smoothed by eliminating any distorting information. Endoscopic images from a WCE examination are prone to misleading content. Hardware limitations (quality of the image sensor and lens, non-adjustable light source) and adverse filming conditions (non-uniform lighting, reflections of the light on intestinal juices and lens cover, peptic content) are likely to cause high levels of noise to reside in total or part of the image (e.g., underexposed). To address this issue, we apply BEEMD analysis and each image is decomposed in eight 2D IMFs and residue. The first two IMFs contain the high frequency components of the image, i.e., the noise that may exist. Therefore, they are discarded and not utilized in the subsequent analysis and for image reconstruction. Figure 8 presents a worst case scenario, where artificial high level noise was added to an ulcer image. The distorted image is decomposed with BEEMD into eight IMFs and residue. The result (reconstructed image) proves that BEEMD is capable of dealing successfully with extreme cases of noise. Sheer

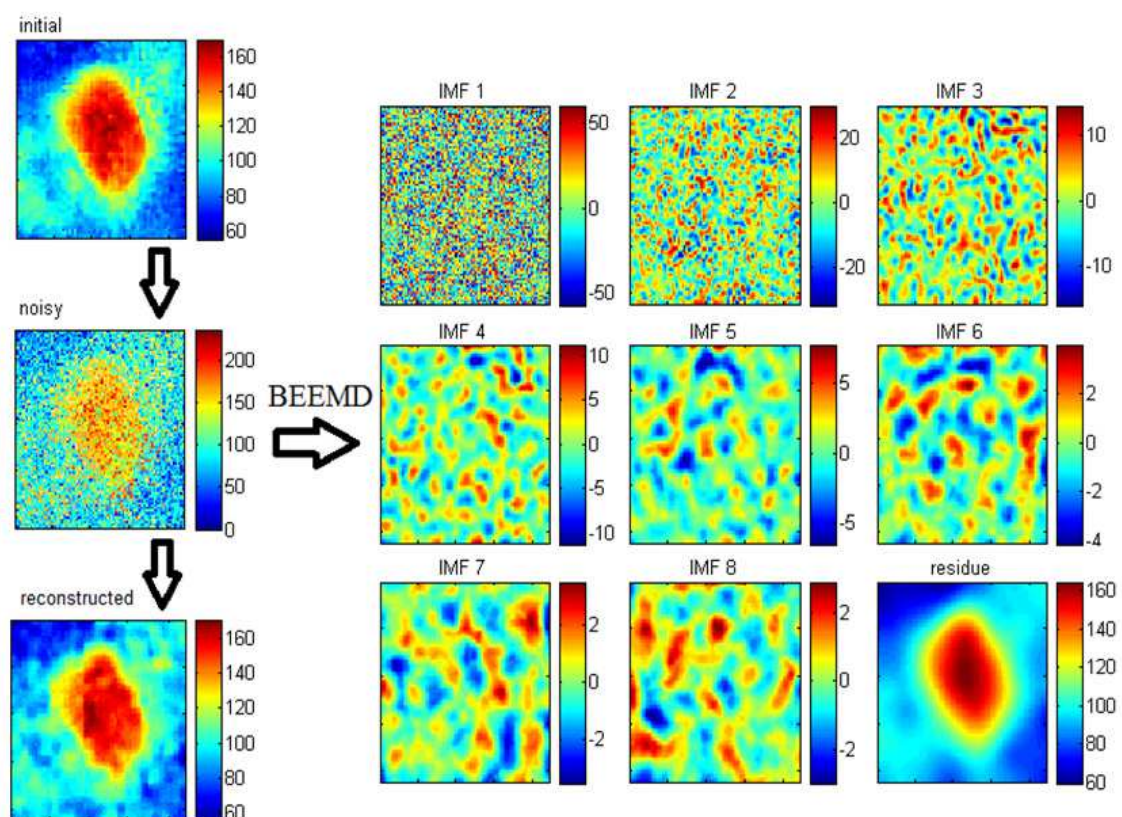


Fig. 8. Ulcer image with high-level, artificial noise decomposed in 8 IMFs plus residue and purified by BEEMD analysis.

noise reduction would be achieved by extracting three or four IMFs only. However, we opted for eight, since our target is to decompose the image to its components towards examining how intestinal information is distributed on a broad range of frequency scales and create a new, reconstructed image that reveals more efficiently ulcer texture information.

The motive for using BEEMD instead of other denoising techniques, such as Gaussian filter or wavelets, lies on the characteristics of the WCE images and the properties of BEEMD. The spatial characteristics of noise in WCE images and the spatial-frequency information representation of BEEMD, combined with its adaptive-to-the-data nature, provides a great advantage over a simple Gaussian filter. Moreover, ulcer regions are characterized by many and varying appearances and irregular shapes and sizes and do not have strong directional elements. Consequently, a tool, free from directional limitations, that permits multi-scale analysis is essential. Wavelet analysis has poor orientation selectivity (horizontal, vertical, diagonal) rendering BEEMD as a more efficient option.

5.3 AR-DLac scheme

In order to follow the WCE image characteristics and focus upon the ones that mostly relate to ulcer, an AR approach was developed. The aforementioned capabilities of EMD were exploited by developing a new DLac-based approach for the optimized selection of IMFs that correspond to ulcer characteristics of a WCE image. Towards this direction, DLac analysis is applied to every IMF of a decomposed image. The selected IMFs are used either to reconstruct a new image (R-case), or provide separate images (NR-case) that represent specific modes of oscillations coexisting in the initial WCE image. Apart from the optimal IMF selection, we are able to investigate how ulcer texture information are distributed across the frequency scales of WCE images.

5.3.1 Proposed DLac analysis

The great advantage of DLac is the ability to perform texture analysis in various scales. The coarseness of the scale is primarily determined by the size of window w , which designates the size of the neighbourhood for box mass calculation; the greater the window, the coarser the analysis scale. In the case of ulcer tissue recognition, a multi-scale texture analysis is required considering the great variability in size and appearance of ulcer regions. In this context, DLac is calculated for a variety of window sizes, given a constant, relative small box size r , in order to achieve pattern analysis at different scales, while identifying slight variations in neighbouring pixels (due to small value of r). An example of DLac- w ($r=3$, $w=4-30$) curves that correspond to images b, d, e and f from Fig. 1 is given in Fig. 9a. The curves are distinct, however, obvious discrimination is not achieved. To deliver greater differentiation between the curves an identical reference level has to be secured (Hadjileontiadis, 2009). Thus, DLac- w curves are normalized to the DLac value that corresponds to the smallest w . The resulting curves (Fig. 9b) provide quite clear discrimination between the four patterns. From now on, any reference to DLac- w curves implies normalized curves.

5.3.2 Optimized IMF selection

The selection of optimum IMFs is based on the characteristics of DLac- w curve of each IMF. The motive for such an approach lies in the concept that IMFs with possible useful texture

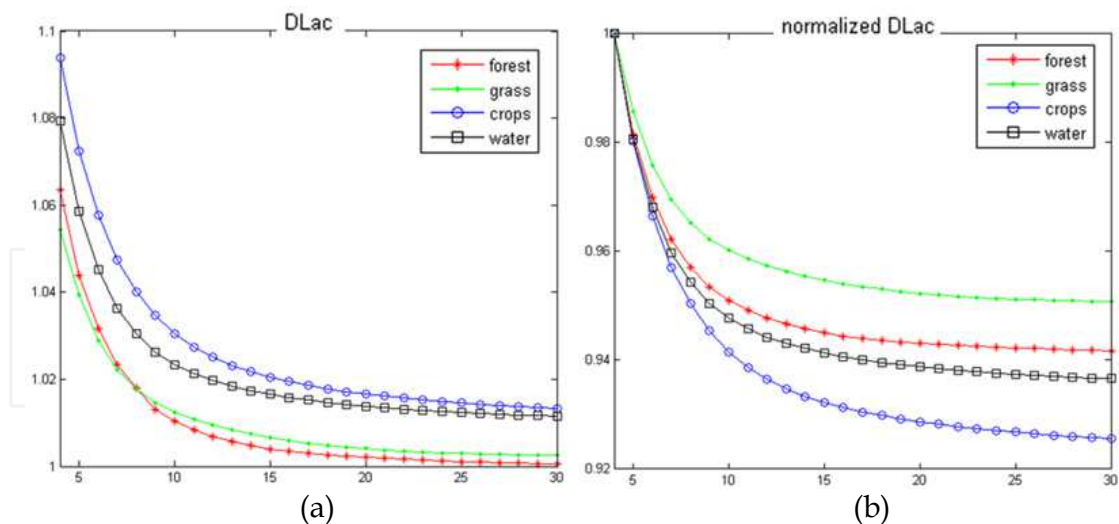


Fig. 9. DLac (a) and normalized DLac (b) curves for various window sizes (4 to 30 pixels) for images b, d, e and f from Fig. 1.

information should provide DLac-w curves that bear resemblance to the curves estimated on ulcer images. In this context, it has been observed that the slope of DLac-w curves of ulcer images lies within specific limits for the majority of ulcer cases. This observation led us to a slope-based criterion for IMF selection. The IMFs that provide DLac curves with slopes within the limits, specified by DLac curves of ulcer images, were selected. Figure 10 shows the selection probability of each IMF. According to the diagram, IMF5, IMF6 and IMF8 were selected for the majority of images implying that the information included in these IMFs should be taken under consideration.

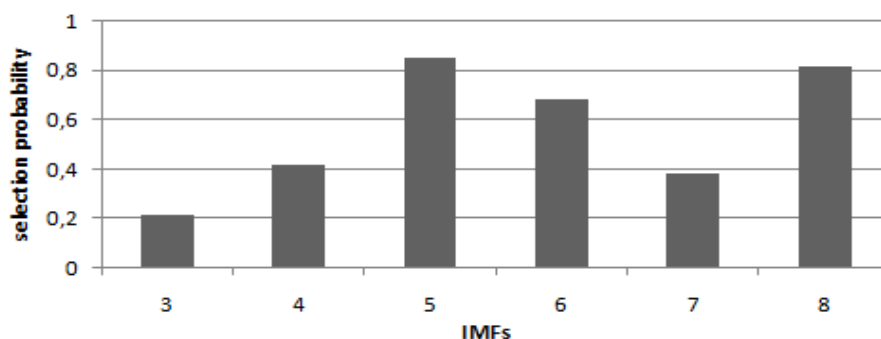


Fig. 10. Selection probability for each IMF.

5.3.3 DLac-based feature vector

In image pattern detection applications, feature vector (FV) is the set of features that characterize and represent an image and are utilized for the discrimination between various patterns. The DLac-based FV extraction was implemented in two different approaches, following the R-case and NR-case scenario. From a general perspective, the previously described DLac-w curve is used to form the FV. In our approach DLac-w curve is calculated for $w=5-30$ pixels. These 26 DLac values consist an extensive FV, subject to the "curse of dimensionality". The essence of reducing the feature space dimension without omitting any crucial information introduces the concept of modelling DLac-w curves with another

function $L(w)$. The normalized DLac- w curves in Fig. 9b expose an attitude that bears resemblance to the one of hyperbola. On this ground, the function

$$L(w) = \frac{a}{w^b} + c, \quad w=[5-30], \quad (5)$$

was chosen to model the normalized DLac- w curves (Hadjileontiadis, 2009). Parameter a represents the concavity of hyperbola, b portrays the convergence of $L(w)$, and c is the translational term. The best interpretation of DLac- w by the model $L(w)$ is computed as the solution of a least squares problem where parameters a , b , c are the independent variables. Parameters a , b , c embody the global behaviour of the DLac curve, i.e., all the substantial information. However, preliminary studies have shown that local behaviour of DLac curve is also important in ulcer tissue classification. Consequently, FV consists of parameters a , b , c plus five DLac values that correspond to the five smallest values of w (i.e., $L(6) - L(10)$; $L(5)$ is discarded as it always equals to one due to normalization). The values $L(6) - L(10)$ were selected empirically after exhausting experiments. In this manner, FV embodies both local and global trend of DLac curve achieving a significant size reduction (eight rather than 26 values).

More specifically, in R-case scenario the selected IMFs and the residue recombine a new image on which the DLac- w curve is calculated and FV is extracted (FV^R) as described above. In NR-case scenario, the final FV (FV^{NR}) contains the FV from each selected IMF (FV_i , $i=3$ to 8). However, different number of IMFs is selected for every image with the subsequent problem of changing FV size. To address this issue, FV is designed to include the FVs from IMFs 5, 6 and 8 (i.e., $FV^{NR} = \{FV_5, FV_6, FV_8\}$) which are the most frequently chosen IMFs (Fig. 10) for all images in the dataset, implying that they contain the majority of beneficial information. Last but not least, the ability of texture information of each individual IMF to discriminate ulcer from normal images is investigated. In this case, the final FV (FV^{indiv}) consists of the FV from an individual IMF, different each time, i.e. $FV^{indiv} = FV_i$ for $i=1$ to 8. IMFs 1 and 2 are included, despite their noise contamination, for an overall assessment.

5.4 Classification

The last step of ulcer detection scheme is the classification procedure. This procedure involves the classification of extracted FVs into healthy/ulcerous and is accomplished by algorithms called "classifiers". The target of a classifier is to identify the population (e.g., healthy or abnormal) to which a FV belongs on the basis of a training set of FVs whose population is already known. It is usual that 90% of the sample dataset is used for training the classifier and 10% for testing. This procedure is repeated ten times (10-fold cross validation) with random training and test sets in order to acquire more accurate results. The classification performance is measured with the aid of accuracy (acc.), sensitivity (sens.) and specificity (spec.) indexes. The average acc., sens. and spec. are obtained in case of 10-fold cross validation technique. Various classification algorithms have been proposed in the literature. For an extensive evaluation of the classification performance of the proposed AR-DLac scheme, the widely used classification algorithms, i.e., LDA (Linear Discriminant Analysis), QDA (Quadratic Discriminant Analysis), MD (Mahalanobis Distance) (Krzanowski, 2000), and SVM (Support Vector Machine) (Cristiani & Shawe-Taylor, 2000), were adopted.

6. Experimental phase

The WCE images used in this study for the development and assessment of the proposed approach were drawn from six patients with ulcerous diseases, such as unexplained ulceration, ulceration from NSAID, ulcerative colitis and Crohn's diseases, who have undertaken a WCE examination in NIMTS Gastroenterology Clinic in Athens, Greece. The examinations were conducted with Pillcam SB (Given Imaging) WCE system. Rapid Reader 6.0 software (Given Imaging) was employed to export the images from the video sequence.

The dataset collected consists of 87 ulcer and 87 normal images. An example of the two categories is given in Fig. 11. The images were obtained by manual segmentation of the initial, complete WCE images. Two gastroenterologists reviewed the endoscopic video and manually isolated regions of interest (ROI), as the ones shown in Fig. 11, according to their expertise and upon agreement. It must be highlighted that the 87 ulcer images were obtained from 87 different events (ulcer regions) to achieve the lowest possible similarity. Furthermore, the normal images include both simple and confusing healthy tissue (folds, villus, bubbles etc.) in order to hamper the discrimination process. The ROI for the normal images varies from 110x110 to 220x220 pixels whereas the crop area of the ulcer images depends on the size, shape and position of the ulcer. The variety in ROI sizes does not affect the tissue discrimination procedure, since the feature vectors extracted from the images are utilized as the basis for comparison instead of the images themselves.



Fig. 11. An example of ulcerous (left) and normal (right) region of interest.

7. Results and discussion

The performance of the proposed AR-DLac scheme is evaluated through the experimental results derived from the application of the introduced approach to the dataset described in §6. To this end, results from every individual IMF analysis as well as results from both AR-DLac implementation scenarios (i.e., R-case and NR-case) are presented in this section.

7.1 Individual IMFs

Table 1 tabulates the classification performance achieved by the texture information extracted from each individual IMF ($FV^{indiv}=FV_i$, where FV_i is the feature vector constructed from IMF $_i$ as described in §5.3.3) for all classifiers. The highest classification rates obtained for each IMF are noted in bold. The format $\% \pm \%$ corresponds to mean acc., sens. and spec. \pm standard deviation.

The low classification rates for IMFs 1-2 denote their inefficiency in discriminating between ulcer and normal tissue. The performance of IMF1, in terms of classification accuracy, ranges

from 51.9% to 61.3%, while the one of IMF2 varies from 53.3% to 62.0%. The sensitivity index is even lower (up to 29.1 percentage points) for the majority of classifiers (i.e., LDA, QDA and SVM). This performance implies that the texture information that lies in IMFs 1 and 2 is not eligible for ulcer detection. This behaviour is consistent with the concept of noise “contamination” of IMF1-2 and validates the noise reduction procedure described in §5.2 and illustrated in Fig 8. IMFs 1-2 contain the high frequency components of the image (i.e., the noise) and, therefore, should be discarded. On the contrary, the classification accuracy of IMF3-8 is 24.8% to 35.5% improved. IMF3 and IMF5 exhibit the lowest (77.4%) and highest (84%) performance (in terms of accuracy), respectively. Despite the superior classification rates, the performance of individual IMFs indicates that texture information that resides in a single image component is inadequate for efficient ulcer detection. Additionally, low classification sensitivity (<76%) suggests extensive misidentification of ulcer regions as healthy. It should be highlighted that IMFs 5, 6 and 8, that are the most commonly selected IMFs (Fig. 10) in IMF selection procedure, deliver the three highest classification accuracy rates among the IMFs. The convergence of these results testifies the optimal IMF selection procedure.

As far as the classification algorithms are concerned, the results in Table 1 imply that the most efficient classifiers include SVM and QDA. SVM achieves the best performance for the majority of IMFs (1-4, 8) due to its more advanced nature. However, the capabilities of QDA should not be underestimated since it exhibits 4.6, 5.7 and 4.8 percentage points higher classification accuracy than SVM for IMF5-7. LDA also proves competent, delivering slightly inferior performance. At last, MD is the most inappropriate classifier for our approach. The extremely high classification sensitivity (up to 99.2% for IMF6) in conjunction with the extremely low classification specificity (down to 15.6% for IMF6) denote over fitting to ulcer texture information.

Classifier		IMF							
		1	2	3	4	5	6	7	8.
LDA	Acc.	55.1±1.7	58.7±1.7	76.9±0.9	78.9±0.7	81.6±0.6	80.0±1.1	78.7±1.0	82.3±0.8
	Sens.	35.9±2.4	51.8±2.4	71.1±1.4	71.3±1.4	70.4±0.9	72.2±1.7	73.4±1.5	82.1±1.4
	Spec.	74.4±2.1	65.5±2.4	82.8±1.4	86.5±0.7	92.7±1.1	87.7±1.6	83.9±1.4	82.5±0.7
QDA	Acc.	59.5±0.8	59.9±1.4	77.1±0.9	79.7±0.7	84.0±0.9	78.2±0.8	79.5±1.3	80.5±0.9
	Sens.	30.4±1.4	42.3±2.2	66.2±1.4	64.9±1.1	72.0±1.3	67.1±1.6	74.0±1.9	65.7±1.5
	Spec.	88.6±1.1	77.5±1.7	88.1±1.5	94.4±0.9	96.0±1.2	89.2±0.6	85.1±1.9	95.3±1.1
MD	Acc.	51.9±0.7	53.3±1.4	61.2±1.1	66.3±1.0	61.3±1.0	57.4±1.4	62.4±1.1	68.5±1.1
	Sens.	98.3±0.8	96.6±1.2	93.8±1.0	93.8±1.0	97.1±0.9	99.2±0.9	98.3±0.9	96.5±1.0
	Spec.	5.6±1.3	10.0±2.7	28.5±1.9	34.6±1.9	25.5±1.8	15.6±2.5	26.5±2.1	40.5±1.9
SVM	Acc.	61.3±1.6	62.0±1.5	77.4±1.1	79.8±1.0	79.4±0.8	72.5±1.1	72.7±1.1	82.5±0.5
	Sens.	42.9±2.0	59.8±1.8	74.2±1.2	75.9±1.3	74.3±1.0	64.1±1.6	62.4±1.3	67.7±0.9
	Spec.	79.8±2.2	64.2±2.6	80.5±1.6	83.5±1.6	84.5±1.3	80.9±1.3	83.1±1.7	93.3±1.0

Table 1. Mean classification accuracy, sensitivity and specificity (%) for each individual IMF (FV_i , $i=1$ to 8), for all classifiers (LDA, QDA, MD, SVM).

7.2 Reconstruction (R-case) – Non Reconstruction (NR-case) scenarios

The proposed AR-DLac scheme, thoroughly described in §5.3, selects the optimum IMFs. In the reconstruction scenario (R-case) the selected IMFs and the residue reconstruct a new image from which the FV is extracted, while in non reconstruction scenario (NR-case) the FVs from the selected IMFs are concatenated in order to form the final FV. The results of both scenarios are tabulated in Table 2, for all classifiers. The best classification rates for each implementation scenario are notated in bold. The format %±% corresponds to mean acc., sens. and spec. ± standard deviation.

Classifier	Implementation scenario					
	R-case			NR-case		
	Acc.	Sens.	Spec.	Acc.	Sens.	Spec.
LDA	95.5±0.5	94.8±0.8	96.2±0.4	89.2±0.9	84.3±1.7	94.1±0.4
QDA	95.8±0.6	93.9±1.1	97.7±0.3	91.2±0.9	86.2±1.3	95.9±1.1
MD	96.3±0.2	96.0±0.1	96.6±0.6	78.7±1.4	98.3±0.9	58.3±2.7
SVM	96.7±0.6	96.5±0.3	96.9±0.9	89.7±0.8	87.5±1.0	91.9±0.9

Table 2. Mean classification rates (%) for both R-case and NR-case scenarios, for all classifiers (LDA, QDA, MD, SVM).

The most efficient performance of the proposed AR-DLac scheme is delivered in R-case scenario where the classification accuracy reaches 96.7% by exploiting SVM classifier. However, the difference between the most (SVM) and the least (LDA) efficient classifier is only 1.2 percentage points, in terms of accuracy, implying that the features extracted by the proposed analysis are quite robust, exhibiting advanced overall performance regardless of the classification algorithm engaged. It is also remarkable the fact that the high accuracy rate is accompanied by high and relatively consistent rates for both sensitivity (96.5%) and specificity (96.9%). These results indicate that AR-DLac scheme is capable of equally recognising ulcer and normal data without exhibiting bias towards a specific pattern. This behaviour applies to all examined classifiers since the difference between sensitivity and specificity does not exceed 2.6 percentage points.

The classification results of the NR-case, suggest inferior performance of the AR-DLac scheme during the non reconstruction scenario. The most effective classifier for NR-case is QDA delivering 91.2% accuracy, 86.2% sensitivity and 95.9% specificity. These rates, compared to those of R-case, are 5.5, 10.3 and 1.0 percentage points lower, respectively. Even the worst scenario for R-case (LDA classifier) achieves 4.3 percentage points higher accuracy than QDA in NR-case. Moreover, the balance between sensitivity and specificity rates deteriorated ranging from 4.4 (for SVM) to 40 (for MD) percentage points. MD, as in the individual IMF case, fails to recognize correctly the normal images since the specificity rate is 58.3%. The divergence in performance between R-case and NR-case indicates that the recomposed image by the optimal IMFs and the residue represents more efficiently the intestinal texture information than the individual components of the image. This may be explained by the fact that in NR-case the trend of the image (residue) is ignored. Moreover, the fact that FV^{NR} includes 3 IMFs \times 8 features = 24 features in total (33% larger than FV^R) may also affect the classification performance.

The comparison of the results in Tables 1 and 2 denotes the inability of a single IMF to separate ulcer from normal images. R-case and NR-case deliver 12.7 and 7.2 percentage points improved classification accuracy compared to the most effective IMF (i.e., IMF5), respectively. The superiority of NR-case suggests that the utilization of a group of individual IMFs is more fruitful than standalone IMF exploitation.

8. Overall perspective and future work

The aforementioned experimental results highlight the potential of the proposed scheme towards ulcer and healthy intestinal tissue discrimination. The optimum image components (IMFs) that contain the majority of texture information include IMFs 5, 6 and 8. Individual IMFs score up to 84% classification accuracy, while their exploitation as a group enhances the detection rate up to 91.2%. On the contrary, the refined image reconstruction process achieves 96.7% successful tissue identification. When compared with other approaches, the proposed scheme seems to be more effective exhibiting increased classification ability by using a smaller feature vector. One of the most efficient ulcer detection approaches (Kodogiannis *et al.*, 2007b), used as a comparison baseline, employs 54 features (instead of 8) and results in 94.5% accuracy when applied to our dataset (Charisis *et al.*, 2011).

In spite of the promising performance of the proposed scheme, there are still some issues for improvements that should be taken under consideration for its use in a future computer aided diagnosis system. Firstly, the number of ulcer and normal images should be increased in order to secure maximum diversity between the ulcer cases, develop more robust algorithms and obtain more accurate conclusions. Secondly, automatic segmentation of the regions of interest (ROI) is mandatory. In our approach, WCE images are manually cropped to the ROI. A potential solution is to divide each WCE image (576x576) into small patches (64x64) and choose the patches that depict mucosa. These patches contain almost all possible ROI by covering the most valid area of the original WCE image. At last, the computational cost of the proposed techniques should be revised. In this work, the introduction of a real time application was not our objective. In this context, the computational cost of the current unoptimized MATLAB code is 9.3 seconds per ROI, considering an average size of 145x145 pixels. BEEMD analysis consumes 83.4% of this time while DLac analysis and classification absorb 16.2% and 0.4%, respectively. When focusing on real time application, dedicated hardware and programming languages, more efficient implementation algorithms (for BEEMD and DLac) and multithreading programming should be considered.

9. Conclusion

Wireless capsule endoscopy (WCE) is a novel, non-invasive form of endoscopy that has started a new era for the visual inspection of the entire small bowel. A WCE system consists of a pill-shaped, wireless capsule that the patient swallows. The capsule, propelled by the natural bowel movements, captures and transmits images from the internal mucous membranes, along its journey through the digestive tract. Despite the revolution WCE has introduced, there are several limitations that pose serious questions about the competency of WCE compared to probe gastroscopy and colonoscopy. Some of the major challenges include camera speed/quality, power supply, controllable manoeuvring and interventional capabilities. Significant research is conducted towards this direction, various approaches have been proposed and the first achievements have emerged. A new capsule equipped

with two cameras and increased battery life has been developed for colon and esophagus examination. Magnetically remote controlling and wireless power transmission concepts are in experimental phase. Apart from the hardware-oriented limitations and approaches there is a major issue concerning the vast amount of data produced by a WCE examination. The optimal WCE needs to contain a computerized system for automatic detection of pathologies such as ulcer and polyps in order to overcome the drawback of time-consuming reviewing of the video (Fireman, 2010). In this context, researchers aim to develop automatic diagnosis systems. The main contribution of this work is the presentation of a novel tool for WCE image analysis and classification by exploiting color-texture features. This color-texture perspective was inspired by the one the gastroenterologist usually adopts in clinical practice for successful diagnosis of pathologies and, especially, ulcer. The proposed AR-DLac scheme is based on the ingenious combination of BEEMD and DLac, applied on the green component of WCE images in order to identify ulcerations. BEEMD, apart from an adaptive image denoising tool, was exploited to reveal the intrinsic components (IMFs) of the images in order to achieve data driven, adaptive image refinement (AR), boost the distinctness between normal and ulcer regions and facilitate DLac analysis to extract efficient texture characteristics. AR entailed optimum IMF selection, based on the structure patterns of IMFs disclosed by DLac. The optimum IMFs were used either to reconstruct a new, refined image, or provide separate images. The proposed AR-DLac approach was evaluated on selected WCE images, captured from patients, depicting ulcer and healthy tissue. Experimental results have shown that AR-DLac scheme exhibits quite satisfactory overall classification performance. Intestinal texture information is distributed along IMFs 3 to 8; thus, the utilization of a single IMF for the detection procedure is not recommended. The classification performance of individual IMFs does not exceed 84% (classification accuracy), with IMF5 being the most efficient. When individual images (i.e., optimum IMFs) are employed (non reconstruction case) the performance improves and accuracy reaches 91.2%. However, the best results are delivered in the reconstruction case, where accuracy, sensitivity and specificity exceed 96.5%. The advanced overall classification performance of AR-DLac approach paves the way for its use in a provisional automatic diagnosis system.

10. References

- Adler, S.N. & Metzger, Y.C. (2011). PillCam COLON capsule endoscopy: recent advances and new insights, *Therapeutic Advances in Gastroenterology*, Vol.4, No.4, pp. 265-268
- Allain, C. & Coitre, M. (1991). Characterizing the lacunarity of random and deterministic fractal sets, *Physical Review A*, Vol.44, No.6, pp. 3552-3558
- Ameling, S.; Wirth, S.; Paulus, D.; Lacey, G. & Vilarino, F. (2009). Texture-based polyp detection in colonoscopy, *Proc. of Bildverarbeitung fur die Medizin 2009*, pp. 364-350, Berlin, Germany, March 22-25, 2009
- Aronott, I.D.R. & Lo, S.K. (2004). The clinical utility of wireless capsule endoscopy, *Digestive Diseases and Sciences*, Vol.49, No.6, pp. 893-901
- Barkin, J.S. & Friedman, S. (2002). Wireless capsule endoscopy requiring surgical intervention: the world's experience, *The American Journal of Gastroenterology*, Vol.97, No.9, pp. S298
- Belvin, ML.; Voderholzer, WA. & Loch, S. (2003). Diagnosing small intestinal strictures: first experience with the M2A patency capsule, *Endoscopy*, Vol.35, Suppl. II, pp. A184

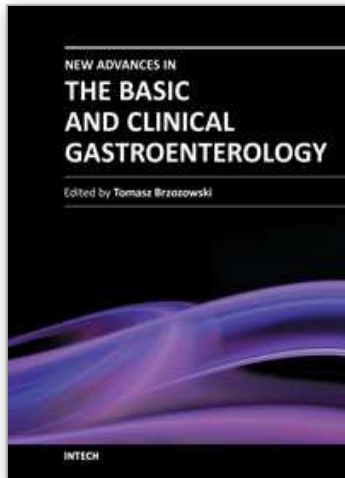
- Berlin, B. & Kay, P. (1969). *Basic Color Terms: Their Universality and Evolution*, University of California Press, ISBN 1-57586-162-3, Berkeley, California
- Bourbakis, N. (2005). Detecting abnormal patterns in WCE images, *Proc. of 5th IEEE Symposium on Bioinformatics and Bioengineering*, pp. 232-238, Minneapolis, U.S.A., October 19-21, 2005
- Capri, F.; Galbiati, S. & Capri, A. (2007). Controlled navigation of endoscopic capsules: Concept and preliminary experimental investigations, *IEEE Trans. on Biomedical Engineering*, Vol.54, No.11, pp. 2028–2036
- Capri, F.; Kastelein, N.; Talcott, M. & Pappone, C. (2011). Magnetically Controllable Gastrointestinal Steering of Video Capsules, *IEEE Trans. on Biomedical Engineering*, Vol.58, No.2, pp. 231-234
- Carta, R.; Thone, J. & Puers, R., Wireless power and data transmission for robotic endoscopic capsules, *Proc. of 12th Mediterranean Conference on Medical and Biological Engineering and Computing*, pp. 232-235, Chalkidiki, Greece, May 27-30
- Cauendo, A.; Rodriguez- Teilez, M.; Hernandez- Duran, M. *et al.* (2003). Evaluation of M2A patency capsule in the gastrointestinal tract: one-capsule preliminary data from a multicentre prospective trial, *Endoscopy*, Vol.35, Suppl.II, pp. A182
- ^aCharisis, V. *et al.* (2010). Abnormal Pattern Detection in Wireless Capsule Endoscopy Images Using Nonlinear Analysis in RGB Color Space, *Proc. of 32nd International Conference of IEEE Engineering in Medicine and Biology Society*, pp. 3674-3677, Buenos Aires, Argentina, August 31- September 4
- ^bCharisis, V. *et al.* (2010). Ulcer Detection in Wireless Capsule Endoscopy Images Using Bidimensional Nonlinear Analysis, *Proc. of 12th Mediterranean Conference on Medical and Biological Engineering and Computing*, pp. 236-239, Chalkidiki, Greece, May 27-30
- Charisis, V.; Hadjileontiadis, L.J.; Liatsos, C.N.; Mavrogiannis, C.C. & Sergiadis, G.D. (2011). Capsule Endoscopy Image Analysis Using Texture Information from Various Color Models, *Computer Methods and Programs in Biomedicine*, under revision.
- Cheifetz, A.S. *et al.* (2006). The risk of retention of the capsule endoscope in patients with known or suspected Crohn's disease, *The American Journal of Gastroenterology*, Vol.101, No.10, pp. 2218-2222
- Coimbra, M. & Silva Cunha, J.P. (2006). MPEG-7 visual descriptors-contributions for automated feature extraction in capsule endoscopy, *IEEE Trans. on Circuits and Systems for Video Technology*, Vol.16, No.5, pp. 628-637
- Cristianini, N. & Shawe-Taylor, J. (2000). *An Introduction to Support Vector Machines and Other Kernel-based Learning Methods*, Cambridge University Press, ISBN 0-52-178019-5, Cambridge, UK
- Dong, P. (2000). Test of a new lacunarity estimation method for image texture analysis, *International Journal of Remote Sensing*, Vol.21, No.17, pp. 3369-3373
- Fireman, Z. (2010). Capsule endoscopy: Future horizons, *World Journal of Gastrointestinal Endoscopy*, Vol.2, No.9, pp. 305-307
- Foster, D.H. *et al.* (1997). Four issues concerning colour constancy and relational colour constancy, *Vision Research*, Vol.37, No.10, pp. 1341-1345
- Foucault, M. (1973). *The Birth of the Clinic: An Archaeology of Medical Perception*, ISBN 0-415-30772-4, Pantheon Books, New York, USA
- Friedman, S. (2004). Comparison of capsule endoscopy to other modalities in small bowel, *Gastrointestinal Endoscopy Clinics of North America*, Vol.14, No.1, pp. 51-60

- Gan, T.; Wu, J.-C.; Rao, N.-N.; Chen, T. & Liu, B. (2008). A feasibility trial of computer-aided diagnosis for enteric lesions in capsule endoscopy, *World Journal of Gastroenterology*, Vol.14, No.45, pp. 6929-6935
- Gao, M.; Hu, C.; Chen, Z.; Zhang, H. & Liu, S. (2010). Design and Fabrication of a Magnetic Propulsion System for Self-Propelled Capsule Endoscope, *IEEE Trans. on Biomedical Engineering*, Vol.57, No.12, pp. 2891-2902
- Gefen, Y.; Meir, Y.; Mandelbrot, B.B. & Aharony, A. (1983). Geometric implementation of hypercubic lattices with noninteger dimensionality by use of low lacunarity fractal lattices, *Physical Review Letters*, Vol.50, No.3, pp. 145-148
- Hadjileontiadis, L.J. (2009). A texture-based classification of crackles and squawks using lacunarity, *IEEE Trans. on Biomedical Engineering*, Vol.56, No.3, pp. 718-732
- Haralick, R.M.; Shanmugam, K. & Dinstein, I. (1973). Textural features for image classification, *IEEE Trans. on Systems, Man and Cybernetics*, Vol.3, No.6, pp. 610-621
- Huang, N.E. *et al.* (1998). The empirical mode decomposition and the Hilbert spectrum for nonlinear and non-stationary time series analysis, *Proc. of Royal Society of London A*, Vol.454, No.1971, pp. 903-995
- Iakovidis, D.K.; Maroulis, D.E. & Karkanis, S.A. (2006). An intelligent system for automatic detection of gastrointestinal adenomas in video endoscopy, *Computers in Biology and Medicine*, Vol.26, No.10, pp. 1084-1103
- Iddan, G.; Meron, G.; Glukhovsky, A. & Swain, P. (2000). Wireless capsule endoscopy, *Nature*, Vol.405, No.6785, pp. 417-417
- Julesz, B. (1975). Experiments in the visual perception of texture, *Scientific American*, Vol. 232, No.4, pp 34-43
- Karkanis, S.A.; Iakovidis, D.K.; Maroulis, D.E.; Karras, D.A. & Tsivras, M. (2007). Computer-aided tumor detection in endoscopic video using color wavelet features, *IEEE Trans. on Information Technology in Biomedicine*, Vol.7, No.3, pp. 142-151
- ^aKodogiannis, V.S.; Boulougoura, M.; Lygouras, J.N. & Petrounias, I. (2007). A neuro-fuzzy-based system for detecting abnormal patterns in wireless-capsule endoscopic images, *Neurocomputing*, Vol. 70, No.4-6, pp. 704-717
- ^bKodogiannis, V.S.; Boulougoura, M.; Wadge, E. & Lygouras, J.N. (2007). The usage of soft-computing methodologies in interpreting capsule endoscopy, *Engineering Applications of Artificial Intelligence*, Vol.20, No.4, pp. 539-553
- Krzanowski, W.J. (2000). *Principles of multivariate analysis: A user's perspective*, Oxford University Press, ISBN 0-19-850708-9, New York, USA
- Li, B. & Meng, M.Q.-H. (2007). Analysis of the gastrointestinal status from wireless capsule endoscopy images using local color feature, *Proc. of 2007 International Conference on Information Acquisition*, pp. 553-557, Jeju, Korea, July 8-11, 2007
- ^aLi, B. & Meng, M. Q.-H. (2009). Computer-based detection of bleeding and ulcer in wireless capsule endoscopic images by chromaticity moments, *Computers in Biology and Medicine*, Vol.39, No.2, pp. 141-147
- ^bLi, B. & Meng, M. Q.-H. (2009). Texture analysis for ulcer detection in capsule endoscopy images, *Image and Vision Computing*, Vol.27, No.3, pp. 1336-1342
- Liao, Z.; Gao, R.; Xu, C. & Li, ZS. (2010). Indications and detection, completion, and retention rates of small-bowel capsule endoscopy: a systematic review, *Gastrointestinal Endoscopy*, Vol.71, No.2, pp. 280-286

- Lorenz, R.; Jorysz, G. & Classen, M. (1993). The value of endoscopy and endosonography in the diagnosis of the dysphagic patient, *Dysphagia*, Vol.8, No. 2, pp. 91-97
- Magoulas, G. (2006). Neuronal networks and textural descriptors for automated tissue classification in endoscopy, *Oncology Reports*, Vol.15, pp. 997-1000
- Maieron, A. *et al.* (2004). Multicenter retrospective evaluation of capsule endoscopy in clinical routine, *Endoscopy*, Vol.36, No.10, pp. 864-868
- Mandelbrot, B.B. (1982). *The Fractal geometry of nature*, W. H. Freeman, ISBN 0-7167-1186-9, New York, USA
- Mandelbrot, B.B. (1993). A fractal's lacunarity, and how it can be tuned and measured, In: *Fractals in Biology and Medicine*, T.F. Nonnenmacher, G.A. Losa, and E.R. Weibel (eds.), pp. 8-21, Birkhauser, ISBN 978-3-7643-2989-1, Basel, Switzerland.
- Meredith, A.; Nightngale, J. & Eden, J.K. (2009). Capsule endoscopy: The risk of retention, *Synergy*, July 2009
- Miller, P. & Astley, S. (1992). Classification of breast tissue by texture analysis, *Image Vision Computing*, Vol.10, No.5, pp. 277-282
- Moglia, A.; Menciassi, A.; Dario, P. & Cuschieri, A. (2009). Capsule endoscopy: Progress update and challenges ahead, *Nature Reviews Gastroenterology & Hepatology*, Vol.6, pp. 353-362
- Mylonaki, M.; Fritscher- Ravens, A. & Swain, P. (2003). Wireless capsule endoscopy: A comparison with push enteroscopy in patients with gastroscopy and colonoscopy negative gastrointestinal bleeding, *Gut*, Vol.52, No.8, pp. 1122-1126
- Pennazio, M. (2005). Diagnosis of small-bowel diseases in the era of capsule endoscopy, *Expert Review of Medical Devices*, Vol.2, No.5, pp. 587-598
- Plotnick, R.E.; Gardner, R.H.; Hargrove, W.W.; Prestegaard, K. & Perlmutter, M. (1996). Lacunarity analysis: A general technique for the analysis of spatial patterns, *Physical Review E*, Vol.53, No.5, pp. 5461-5468
- Riccioni, M.E. *et al.* (2003). M2A patency capsule in the evaluation of patients with intestinal stricture: preliminary results, *Endoscopy*, Vol.35, Suppl.II, pp. A6
- Rutgeerts, P. *et al.* (1980). Crohn's Disease of the Stomach and Duodenum: A Clinical Study with Emphasis on the Value of Endoscopy and Endoscopic Biopsies, *Endoscopy*, Vol.12, No.6, pp. 288-294
- Swain, P. (2008). The future of wireless capsule endoscopy, *World Journal of Gastroenterology*, Vol.14, No.26, pp. 4142-4145
- Swain, P. *et al.* (2010). Remote magnetic manipulation of a wireless capsule endoscope in the esophagus and stomach of humans, *Gastrointestinal Endoscopy*, Vol.71, No.7, pp. 1290-1293
- Tuceryan, M. & Jain, A.K. (1998). Texture Analysis, In: *The handbook of pattern recognition and computer vision*, C.H. Chen; L.F. Pau, & P.S.P. Wang, (Eds), 207-248, World Scientific Publishing Co., ISBN 9-810-23071-0, Singapore
- Van Gossum, A. *et al.* (2009). Capsule endoscopy versus colonoscopy for the detection of polyps and cancer, *The New England Journal of Medicine*, Vol.361, No.3, pp. 264-270
- Wang, P.; Krishnan, S.M.; Kugean, C. & Tjoa, M.P. (2001). Classification of endoscopic images based on texture and neural network, *Proc. of 23rd International Conference of the IEEE Engineering in Medicine and Biology Society*, Vol. 4, pp. 3691-3695, Istanbul, Turkey, October 25-28, 2001

- Waterman, M. & Gralnek, I.M. (2009). Capsule endoscopy of the esophagus, *Journal of Clinical Gastroenterology*, Vol.43, No.7, pp. 605-612
- Wu, Z. & Huang, N.E.(2009). Ensemble empirical mode decomposition: A noise-assisted data analysis method, *Advances in Adaptive Data Analysis*, Vol.1, No.1, pp. 1-41
- Wu, Z.; Huang, N.E. & Chen, X. (2009). The multi-dimensional ensemble empirical mode decomposition method, *Advances in Adaptive Data Analysis*, Vol.1, No.3, pp. 339-372
- Xie, J.; Jiang, Y. & Tsui, HT. (2005). Segmentation of kidney from ultrasound images based on texture and shape priors, *IEEE Trans. on Medical Imaging*, Vol.24, No.1, pp. 45-57
- Xin, W.; Yan, G. & Wang, W. (2010). Study of a wireless power transmission system for an active capsule endoscope, *International Journal of Medical Robotics and Computer Assisted Surgery*, Vol.6, No.1, pp. 113-122

IntechOpen



New Advances in the Basic and Clinical Gastroenterology

Edited by Prof. Tomasz Brzozowski

ISBN 978-953-51-0521-3

Hard cover, 546 pages

Publisher InTech

Published online 18, April, 2012

Published in print edition April, 2012

The purpose of this book was to present the integrative, basic and clinical approaches based on recent developments in the field of gastroenterology. The most important advances in the pathophysiology and treatment of gastrointestinal disorders are discussed including; gastroesophageal reflux disease (GERD), peptic ulcer disease, irritable bowel disease (IBD), NSAIDs-induced gastroenteropathy and pancreatitis. Special focus was addressed to microbial aspects in the gut including recent achievements in the understanding of function of probiotic bacteria, their interaction with gastrointestinal epithelium and usefulness in the treatment of human disorders. We hope that this book will provide relevant new information useful to clinicians and basic scientists as well as to medical students, all looking for new advancements in the field of gastroenterology.

How to reference

In order to correctly reference this scholarly work, feel free to copy and paste the following:

Vasileios Charisis, Leontios Hadjileontiadis and George Sergiadis (2012). Enhanced Ulcer Recognition from Capsule Endoscopic Images Using Texture Analysis, *New Advances in the Basic and Clinical Gastroenterology*, Prof. Tomasz Brzozowski (Ed.), ISBN: 978-953-51-0521-3, InTech, Available from: <http://www.intechopen.com/books/new-advances-in-the-basic-and-clinical-gastroenterology/enhanced-ulcer-recognition-from-capsule-endoscopic-images-using-texture-analysis>

INTECH
open science | open minds

InTech Europe

University Campus STeP Ri
Slavka Krautzeka 83/A
51000 Rijeka, Croatia
Phone: +385 (51) 770 447
Fax: +385 (51) 686 166
www.intechopen.com

InTech China

Unit 405, Office Block, Hotel Equatorial Shanghai
No.65, Yan An Road (West), Shanghai, 200040, China
中国上海市延安西路65号上海国际贵都大饭店办公楼405单元
Phone: +86-21-62489820
Fax: +86-21-62489821

© 2012 The Author(s). Licensee IntechOpen. This is an open access article distributed under the terms of the [Creative Commons Attribution 3.0 License](#), which permits unrestricted use, distribution, and reproduction in any medium, provided the original work is properly cited.

IntechOpen

IntechOpen